# Path Loss Analysis and Transceiver Development for Human Body Communication-Based Signal Transmission for Wearable Robot Control

## WEI LIAO[1], KOKI MURAMATSU[2], AND JIANQING WANG [2], (Fellow, IEEE)

[1]School of Electric and Electronic Engineering, Shanghai University of Engineering Science, Shanghai 201620, China
[2]Graduate School of Engineering, Nagoya Institute of Technology, Nagoya 466-8555, Japan

Corresponding author: Jianqing Wang (wang@nitech.ac.jp)

**ABSTRACT** Human body communication (HBC) technology is attracting a lot of attention for monitoring vital data and controlling wearable robot. In this paper, we focused on electroencephalogram (EEG) signal transmission from head to wrist in the 10-60 MHz HBC band. This is based on an idea to transmit an EEG signal to control a wearable robot. First, we clarified the basic transmission mechanism and characteristics using a highly simplified human body model. Next, we performed a detailed path loss analysis by finite difference time domain simulation using an anatomical human body model with various postures. Based on the analysis results, we identified the optimum transmitter position on the head and developed an impulse radio transceiver for verifying the feasibility of the technique. The results show that the developed transceiver can provide a data rate of 10 Mbps and the bit error rate can be kept below $10^{-3}$ for transmitting the EEG signals from the head to the wrist. Experimental validation with a bio-equivalent gel phantom also demonstrated high feasibility of transmitting the EEG signals along the human arm.

**INDEX TERMS** Human body communication, wearable robot control, path loss, impulse radio, transceiver, electroencephalogram signal.

## I. INTRODUCTION

In recent years, research on wireless devices based on human body communication (HBC) has become more and more extensive [1]–[3]. HBC technology uses human body as an effective communication path to transmit data. Since the signal is transmitted along the human body and the radiation generated outside the body is very small, HBC technology is attracting a lot of attention in health care and wearable robot control from the viewpoint of high reliability and high security [4]–[6]. Moreover, in addition to use electromyogram (EMG) signals to control wearable robots such as myoelectric artificial hand, it is expected to use electroencephalogram (EEG) signals to control the wearable robot [7], [8]. A wearable robot usually consists of sensors to detect necessary vital signals and motors to drive the robot. There are many wires between the signal sensors and the motor controllers, which cause many inconveniences.

The associate editor coordinating the review of this manuscript and approving it for publication was Razi Iqbal .

As shown in Fig. 1, wireless connections are promising instead of wires, offering more freedom. Moreover, controlling a wearable robot usually requires multiple EMG or EEG sensors. However, most of the current research is based on the transmission of a single sensor signal, without considering the interaction of multiple sensors working simultaneously. Therefore, elucidating the transmission characteristics of the human body in a multi-sensor environment and realizing real-time signal transmission for wearable robot control are important issues to be solved.

For the frequency bands that can be used for wireless control of wearable robots, one can refer to IEEE 802.15.6 [9]. IEEE 802.15.6 includes the tens of MHz band, 2.45 GHz industrial scientific and medical (ISM) band and ultra-wide band (UWB). UWB can transmit at high speeds over ultra-wide band, but signals are greatly attenuated by the human body. The HBC band has less on-body path loss than other frequency bands because the human body acts almost as a conducting medium in this band [10], [11]. Considering that the frequency components of EMG and EEG signals are
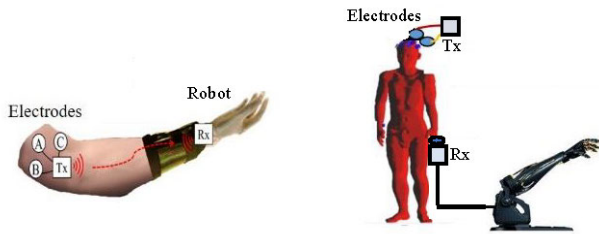
**FIGURE 1.** Concept of wireless control of wearable robot using EMG signal (left) and EEG signal (right).

usually hundreds of hertz, a sampling rate of 2 kHz is reasonable for analog to digital conversion (ADC). In addition, 12-bit quantization is sufficient to convert the analog EMG and EEG signals to digital data. This suggests that a wireless transmission of at least one sensor data requires a data rate of 24 kbps. Wearable robots are typically controlled by a few to a dozens or more EMG or EEG signals, so assuming ten sensors are used, the actual data rate should be at least 240 kbps. A bandwidth of 10-60 MHz is therefore sufficient to transmit the multiple EMG or EEG sensor signals. In addition, this HBC band belongs to the weak radio band in Japan. It is convenient to use because no license is required as long as the radiated electric field strength is less than 500 $\mu$V/m at a distance of three meters [12].

In this study, focusing on transmitting the EEG signals from head to wrist in the 10-60 MHz HBC band, we attempt to derive the transmission characteristics from the transmitting electrodes on the head to the receiving electrodes on the wrist where a robotic hand is assumed to be attached. First, the basic mechanism of transmission is explained using a highly simplified human body model. Then, numerical human body models are built with five typical postures such as standing, walking, sitting, and so on. The transmitting electrodes are assumed in typical EEG signal detection positions on the head, because they can detect and transmit bio-signals at the same time using the same electrode in a time division manner in HBC [13]. By using the finite difference time domain (FDTD) method together with five different posture human body models, the propagation characteristics from the head to the wrist are investigated, and the path loss is derived. Finally, an HBC-based wide band transceiver module is designed and its communication performance is evaluated using the derived path loss characteristics. A transmission experiment using a bio-equivalent phantom is also conducted to show the feasibility of signal transmission from the head to the wrist.

The results will provide new theoretical basis and technical support for HBC-based wearable robot control, and also have important significance for promoting the solution of other related problems in this field.

## II. PROPAGATION CHARACTERISTICS
### A. BASIC MECHANISM AND CHARACTERISTICS
The human tissue is formed by combination of cells in the extracellular fluid. The extracellular fluid, cellular membrane

and intracellular fluid make up tissue. The tissue has a frequency-dependent complex permittivity characteristic. The tissue's permittivity produces a capacitive component, and conductivity produces a resistance component. They are in a parallel form from an equivalent circuit viewpoint. Since each tissue is fundamentally the same structure, the equivalent circuit at the tissue level can be expressed as a parallel circuit of an equivalent resistor $R$ by conductivity and an equivalent capacitor $C$ by permittivity at low frequencies [1]. This suggests that the human body is a lossy dielectric medium.

Wireless control of wearable robots needs to transmit the detected bio-signals along the human body. The human body is first highly simplified as a semi-infinitely large lossy dielectric medium in the x-y plane with relative permittivity $\varepsilon_r$ and conductivity $\sigma$. When a vertical dipole in the z-direction is placed on the surface of the semi-infinitely large lossy dielectric medium, the z-directed electric field on the lossy dielectric medium surface is given by [14]

$$E_z = 2\left[ G_s \frac{jk_0}{d} - \frac{1}{d^2} - \frac{j}{k_0 d^3} \right] e^{-jk_0 d} \tag{1}$$

where $k_0$ is the wave numbers of free space, and $G_s$ is a gain factor to reflect the propagation characteristic along the lossy dielectric medium surface. In Eq. (1), the first term is proportional to the inverse of the surface distance, that is, the $1/d$ term, can be approximately regarded as a wave propagating along the lossy dielectric medium surface, or a surface propagation component. The other two terms ($1/d^2$ and $1/d^3$ terms) in Eq. (1) correspond to the induction and electrostatic field components of the dipole, respectively. The transmission mechanism of on-body communication can be therefore divided into three parts: the surface propagation of the $1/d$ term, the reactive induction of the $1/d^2$ term, and the electrostatic coupling of the $1/d^3$ term. Which term dominates depends on the distance normalized to the wavelength, not the actual propagation distance $d$. That is, it depends on frequency. Given the muscle's $\varepsilon_r$ and $\sigma$, we calculated the path loss as a function of frequency at an on-body communication distance of one meter using (1). Fig. 2 shows the path loss at one meter with respect to 0.05 m. The path loss is almost flat with frequency between 10 and 60 MHz, and is around 80 dB at a distance of one meter. The path loss at 60 MHz is slightly 4 dB less than that at 10 MHz. This path loss calculated using (1) is based on the assumption of propagation along an infinitely large medium plane, so it may be smaller than actual propagation along the human body. However, it can be used as a reference.

Moreover, to clarify the contribution from each term to the received electric field component, the percentages of the three components in the total received electric field strength were calculated. Fig. 3 shows the percentages of the electrostatic component (the $1/d^3$ term) and the percentage of the surface propagation component and the inductive component (the $1/d$ term and $1/d^2$ term), which was calculated using (1) at a distance of one meter. As can be seen from Fig. 3, the electrostatic field component (the $1/d^3$ term) is found to

W. Liao *et al.*: Path Loss Analysis and Transceiver Development for HBC-Based Signal Transmission for Wearable Robot Control
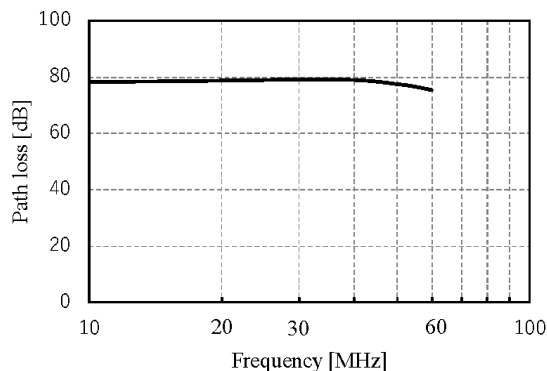
IEEE*Access*



FIGURE 2. Calculated path loss on a semi-infinitely large lossy dielectric medium at a distance of one meter.



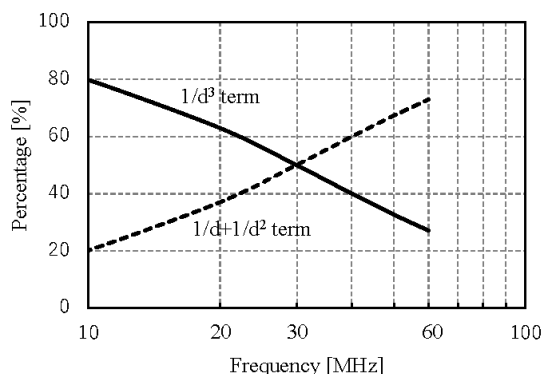FIGURE 3. Percentage of contributions from different signal propagation mechanisms.



FIGURE 4. Human body models for different postures.
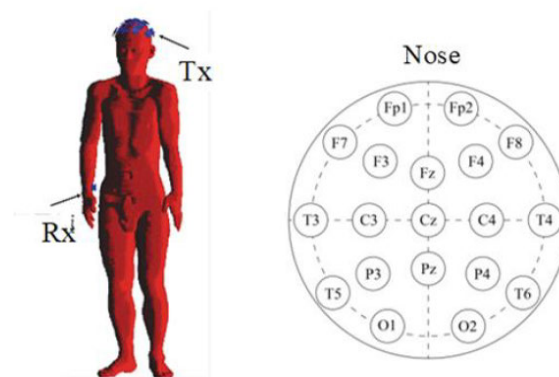


FIGURE 5. Assumed positions of the transmitting electrodes and the receiving electrode.

take more than 50% below 30 MHz and nearly 30% (equal to either the surface propagation component or the inductive component) up to 60 MHz within the total received electric field. This means that the electrostatic coupling is the main transmission mechanism of HBC below 60 MHz. When using this frequency band for wireless control of wearable robots, the transceiver should be designed based on the electrostatic coupling transmission mechanism, and the electrodes should be used to transmit and receive signals instead of antennas.

### B. SIMULATION MODELS AND METHOD
To simulate actual situation of signal transmission from head to wrist, an anatomical human body model was used. The model was developed on the basis of a statistical database of the body dimensions of Asian adults, consisting of 50 tissue types with a spatial resolution of 2 mm [15]. The human body model was further modified to have five different postures such as standing, walking, sitting, working on desk, and sitting on the floor, as shown in Fig. 4. This is because HBC is easy to be affected by body posture and external environment. We therefore need to quantify the variation in path loss with respect to body posture for transceiver design. Based on the basic propagation mechanism of electrostatic coupling, two metal electrodes were used in the transmitter to excite the signal and receiver to detect the signal, respectively.
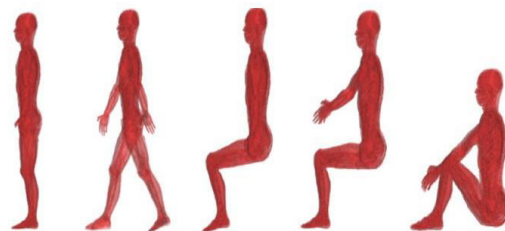
Each electrode was composed of two circular metal plates with a diameter of 30 mm, and the spacing between the two plates was 10 mm. In fact, by introducing a time division scheme, it is also possible to detect the EEG signals using the transmitting electrodes [13]. This means that the transmitting electrodes are used for both HBC signal transmission and EEG signal detection. Therefore, it is reasonable to assume that the transmitting electrodes are set at the same positions as the EEG detection positions on the head.

Fig. 5 shows an overview of the transmitting electrodes (Tx) and receiving electrode (Rx) set on the human body model, and all of the possible positions of the transmitting electrodes on the head are according to the international 10-20 method. They are similar to the positions of electrodes on an EEG helmet. An intersection $C_z$ can be seen between two lines. The first line is from the nose to the back of the head, and the other one is between the two ears. The line connecting the nose and the back of the head is divided into 10%, 20%, 20%, 20%, 20% and 10% to set $F_{pz}$, $F_z$, $C_z$, $P_z$ and $O_z$. The line between the two ears is divided with the same method to set $T_3$, $C_3$, $C_z$, $C_4$ and $T_4$. The left semicircle is divided in $F_{p1}$, $F_7$, $T_3$, $T_5$ and $O_1$. The right semicircle is divided in $F_{p2}$, $F_8$, $T_4$, $T_6$ and $O_2$. The midpoint of $F_7$-$F_z$, $F_8$-$F_z$, $T_5$-$P_z$ and $T_6$-$P_z$ are set as $F_3$, $F_4$, $P_3$ and $P_4$. With this method, almost all areas of the brain are considered. Our basic consideration is to first collect the required EEG signals at different positions to one position on the head, and then transmit the collected EEG signals from that position to a

**IEEE** *Access*

W. Liao *et al.*: Path Loss Analysis and Transceiver Development for HBC-Based Signal Transmission for Wearable Robot Control

wearable robot hand through the human body. The transceiver has multiple inputs. The multiple input signals are converted to one packet, and then the signals are transmitted packet by packet from one position on the head to the wrist.

To analyze the propagation characteristics in the multi-sensor environment, a Gaussian pulse voltage source $v_t(t)$ with signal components mainly between 10 MHz and 60 MHz was used to excite one of the transmitting electrodes on the head and the voltage $v_r(t)$ received at the receiving electrode on the wrist was calculated by the FDTD method. The frequency-dependent permittivity and conductivity of various tissues in the human body were determined based on Gabriel's measurement data [16]. This simulation situation corresponds to that the EEG signals detected by the multiple sensors on the head are first collected by a coordinator placed at one position of the transmitting electrodes, and then transmitted as a packetized signal to the receiver on the wrist by HBC technology. While the signal is transmitted, all detection electrodes are present and affect the propagation characteristics. From the Fourier transforms of $v_t(t)$ and $v_r(t)$, the path loss *PL* between the transmitting and receiving electrodes can be obtained as a function of frequency as follows

$$PL(f)_{dB} = 20 \log_{10} \left[ \frac{F[v_t(t)]}{F[v_r(t)]} \right] \tag{2}$$

where the symbol *F* means the Fourier transform.

### C. SIMULATION RESULTS

Fig. 6 shows the FDTD-calculated path loss at various transmitting electrode positions and different frequencies for the standing posture. It can be seen that the path loss can vary by approximately 25 dB between different transmitting electrode positions and by approximately 30 dB between 10 MHz and 60 MHz. In the frequency band of 10 to 60 MHz, the higher the frequency, the less the path loss is. The path loss at $C_z$ and $F_z$ positions is small. It is known that the path loss in free space increases with frequency. However, the human body is a lossy dielectric object. It has a very high permittivity at MHz band which yields a capacitive coupling between the human body and the external ground. This feature suggests that the body channel looks like a high-pass filter in the 10 - 60 MHz band due to the capacitive return path. This is why the path loss is lower at 60 MHz than that at 10 MHz. This feature is valid below 100 MHz, and can also be confirmed in other literature such as [17], [18]. By using capacitive termination, however, the human body may act as a flat band channel as reported in [19], [20].

Usually, the longer transmission distance leads to higher path loss. However, since the distance is along the body surface with a complicated shape, there may be shadowing between the Tx and Rx. Therefore, the actual path loss will vary over the average path loss. Since the distance between the Tx electrode position on the head and the Rx electrode position on the wrist does not change much, the variation
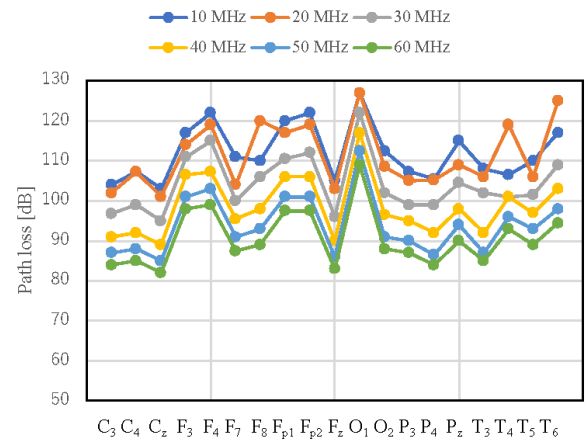


**FIGURE 6.** Calculated path loss at various transmitting electrode positions and different frequencies for the standing posture.
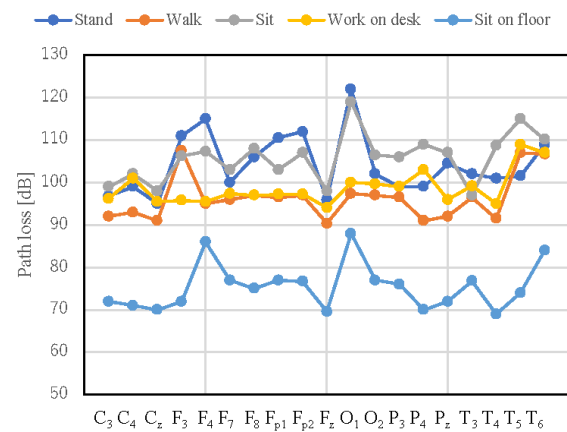


**FIGURE 7.** Effect of postures on the path loss at 30 MHz.

in Fig. 6 is mainly due to the shadowing. In general, the path loss is small when the Tx electrode is at the front of the head.

Fig. 7 shows the effect of posture on the path loss at 30 MHz. The effect is similar for other frequencies from 10 to 60 MHz. From Fig. 7, it can be found that the variation range of path loss may reach 30 dB depending on the posture, and the shadowing increases the path loss significantly. This tendency is the same as in [21] where the reason for path loss variations during different body postures is explained to be due to the limb joints and limb movement. The limb joints produce shadowing and thus increase the path loss. The increase of path loss is proportional to the joint angles. The standing posture can be approximately regarded as a typical posture for investigating the path loss, and the posture sitting on the floor has the lowest path loss.

Since the entire frequency band of 10 to 60 MHz is expected to use for realizing a wide band transmission, the path loss averaged at 10 to 60 MHz was calculated at various transmission electrode positions, and shown in Fig. 8. It can be seen that setting the Tx electrode at the position such as Fz can yield a smaller path loss of about 80 - 100 dB. Moreover, the simulated path loss was obtained from the
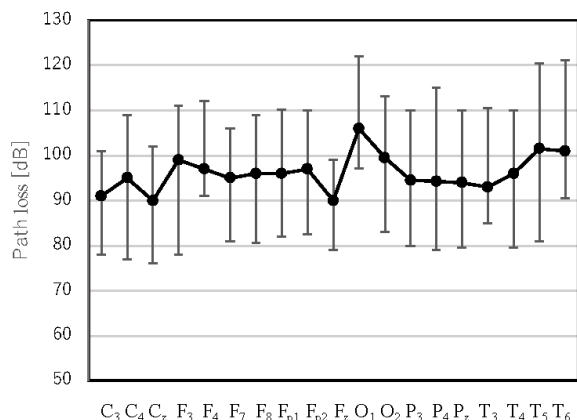
W. Liao *et al.*: Path Loss Analysis and Transceiver Development for HBC-Based Signal Transmission for Wearable Robot Control

**IEEE** *Access*



**FIGURE 8.** Calculated path loss averaged at 10 - 60 MHz at various transmitting electrode positions. The error bars show the variation range due to different postures.

transmitted voltage and the received voltage at the receiving electrode which corresponds to a nearly infinitely large input impedance of receiver. In actual receiver design, however, the input impedance of receiver is usually 50 Ω. Based on our additional simulation result, when the input impedance is changed to 50 Ω, hundreds of times current will flow through the 50-Ω input impedance at the receiver. The received power will be much larger for a 50-Ω input impedance than that for a nearly infinitely large input impedance. This suggests that the path loss will be further improved at least 20 dB when the receiver is designed to have a 50-Ω input impedance. Due to the this reason, the path loss for our considering communication route is about 60 - 80 dB. If the output power of transmitter is set to -10 dBm, a sensitivity of -90 dBm can basically meet the requirement of signal transmission.

Fig. 8 also shows the variation range of path loss due to different postures with error bars. In the considered five postures, the path loss of the standing posture and sitting posture is larger. The upper limit of the path loss in Fig. 8 is mainly determined by either the standing posture or the sitting posture, and the lower limit of the path loss is determined by the posture sitting on the floor. The path loss of walking posture and the path loss of working on desk posture are between the upper and lower limits. This tendency suggests that the signal is easier to transmit when the hand with the receiver is raised forward and upward. To clarify this point, the electric field distributions were calculated and shown in Fig. 9 for the standing and walking postures. It can be seen that the electric field along the arm is significantly strengthened so that a lower path loss from the head to the wrist can be expected. In fact, the electric field strength at the tip of the hand in the walking posture is about 7 dB larger than that in the standing posture.

Moreover, the statistical characteristic of the variation range of path loss due to the posture was analyzed. Fig. 10 shows the cumulative probability distribution of the variation range in unit of dB. It can be seen that the variation range in dB follows normal distribution with a mean
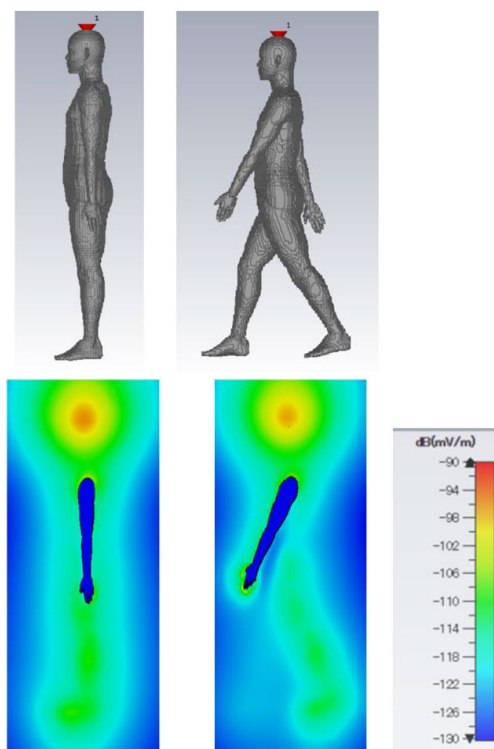


**FIGURE 9.** Electric field distributions at 40 MHz for standing (left) and walking (right) postures in the vertical plane through the left arm.
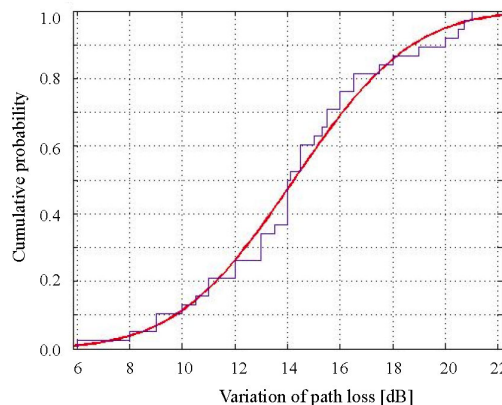


**FIGURE 10.** Cumulative probability distribution of variation range of path loss. The red line is normal distribution.

of 14.2 dB and a standard deviation of 12.2 dB. This should be useful for link budget analysis in transceiver design.

## III. TRANSCEIVER DESIGN

Based on the analysis results of propagation characteristics, an impulse radio (IR) transceiver was designed in the 10 to 60 MHz band from the viewpoint of high speed transmission and low power consumption. Such a transceiver, instead of using electrodes, can also be used for implant communication where signals are transmitted and received using antennas [22]. As the modulation method, multiple pulse position modulation (MPPM) was adopted in which one-bit information is represented by temporal positions of multiple
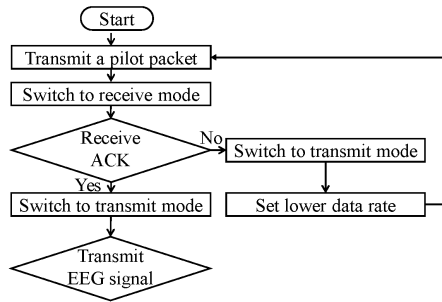
**FIGURE 11.** Flow chart of transceiver with a half-duplex communication function.



**FIGURE 12.** Configuration of the transceiver for transmitting three sensor signals.



**FIGURE 13.** Packet structure.

**TABLE 1.** Specifications of transceiver.

| | |
|---|---|
| Signal sampling frequency | 2 kHz |
| Signal quantification | 12 bits |
| Packet length | 598 bits |
| Duplex | Half-duplex |
| Frequency band | 10 - 60 MHz |
| Band width $B$ | 50 MHz |
| Modulation | MPPM |
| Variable date rate $f_b$ | 20, 10, 5, 2.5, 1.25 Mbps |
| Output power $P_t$ | -10 dBm |
| Receiver amplifier | 40 dB + 40 dB AGC |
| Demodulation | Energy detection |
| Noise figure $N_F$ | 6 dB |

pulses [13], [23]. In IR-MPPM, the data rate can be changed by setting the number of pulses to $L$ and adjusting $L$. Here $L$ is called as spreading ratio. Fig. 11 shows the flow chart of the transceiver with a half-duplex communication function. The transmitting module first sends a pilot packet at a higher data rate and then enters the receive mode to be ready to receive an acknowledgment (ACK) signal. When the transmitting module receives the ACK signal, the current data rate is maintained and packets consisting of EEG signals are transmitted. But if the ACK signal cannot be received, the data rate will be lowered by changing the spreading ratio $L$ to improve communication reliability from the next packet.

The transceiver was designed and implemented in a field programmable gate array (FPGA, Xilinx Spartan-7). Fig. 12 shows the configuration of the transceiver for transmitting three sensor signals to control a wearable robot. With the same configuration, it can be extended to more sensors. The transmitting module consists of four parts: a modulator, a packet generator, a parallel-serial converter, and a data rate switching unit. The EEG signals are quantized by each ADC to 12 bits at a sampling rate of 2 kHz. Each quantized signal is modulated at necessary spreading ratio $L$. The modulated signal is output to the packet generator and stored as a payload. When 16 samples of EMG signals are accumulated, the start bits, headers, and stop bits are added to the payload to generate packets, as shown in Fig. 13, and the generated packets are output chip by chip (pulse by pulse) at a frequency of 20 MHz. After that, a signal with an appropriate data rate or $L$ was selected from the output signal, and a pulse was generated and output by passing it through a band pass filter (BPF) of 10-60 MHz.

Fig. 14 shows the configuration of receiving module. The receiving module employs energy detection as the demodulation method. The received signal is input to the energy detector as discrete data sampled at 150 MHz. After the envelope is extracted by the signal processing unit, it is demodulated into binary digital data and sent to the FIFO (First-In First-Out). After that, the sequence number of the received packet and the packet reception completion flag are output to the transmitting module, and the demodulated payload is converted to analog signal by digital-analog converter (DAC) and send to the controller of wearable robot.
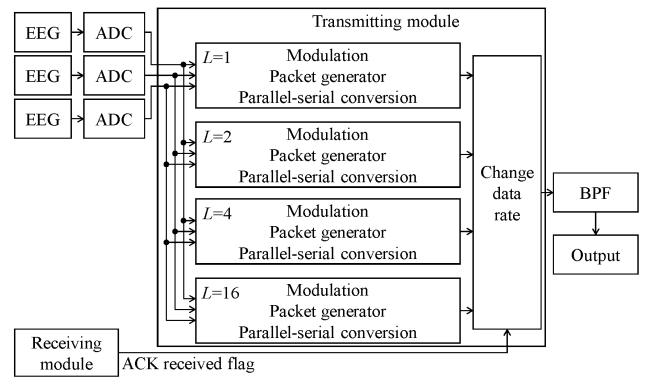
Table 1 summarizes the specifications of the developed transceiver, and Fig. 15 shows its implementation of prototype. By using s smaller FPGA, the transceiver is being developed for 2 cm × 2 cm. In addition, Table 2 compares some typical HBC transceivers [2], [3], [24], [25] for their main performances.

## IV. COMMUNICATION PERFORMANCE EVALUATION

An acceptable bit error rate (BER) level in the physical layer is usually $10^{-3}$ because at this level an error-free communication can be achieved by introducing a forward error correction technique. The communication performance evaluation was therefore performed by choosing BER = $10^{-3}$ as an index. If we take the energy detection duration as the reciprocal of the frequency bandwidth, i.e. $1/B$, the BER $P_e$ can be approximated as [26]
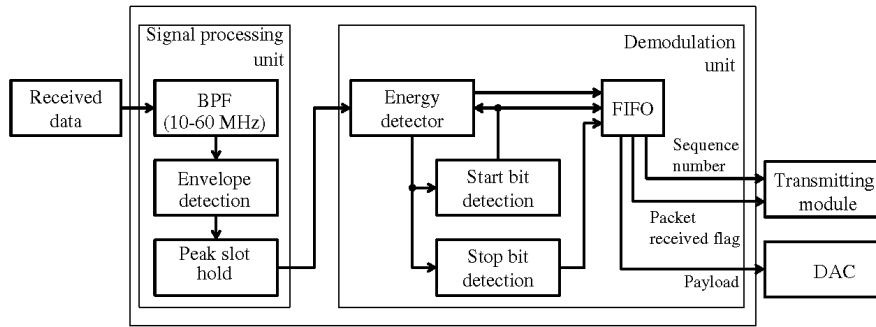
$$P_e = \frac{1}{2}e^{-E_b/2N_0} \tag{3}$$

W. Liao *et al.*: Path Loss Analysis and Transceiver Development for HBC-Based Signal Transmission for Wearable Robot Control

**IEEE** *Access*



**FIGURE 14.** Configuration of receiving module.

**TABLE 2.** Comparison of some typical HBC transceivers.

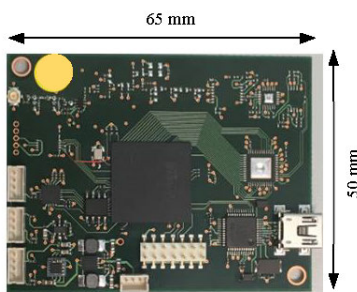| | [2] | [3] | [24] | [25] | This work |
|---|---|---|---|---|---|
| Freq. band | 100-500 KHz | 125 kHz | 5 MHz | 10-70 MHz | 10-60 MHz |
| Modulation | OOK-DSSS | FSK | Electro-optic | PPM-DSSS | IR-MPPM |
| Date rate | 2.4 kbps | 4 kbps | 10 Mbps | 10 Mbps | 20 Mbps |
| Duplex | - | - | - | - | Half |

DSSS: Direct sequence spread spectrum



**FIGURE 15.** Implementation of transceiver.

where $E_b/N_0$ is the energy per bit to noise power spectral density ratio. The noise is mainly considered thermal noise from the front-end amplifier of transceiver. Actually, the human body picks up a lot of environmental interferences, and the actual noise model may be the thermal noise plus the interferences. However, there is no such reported noise model for HBC, and building such a complex noise model is beyond the scope of this study. Therefore, as usual, we assumed an additive white Gaussian noise model in the link budget analysis. This will provide basic communication performance. For interference such as electrostatic discharge (ESD) impulse noise, the developed communication method has shown to significantly improve immunity due to the adoption of the wide band modulation method [23].

From (3), an $E_b/N_0$ of 10.94 dB is required to achieve this BER level, which is named as $E_b/N_{0,Spec}$. By denoting $f_b$ as the data rate and $B$ as the bandwidth, $E_b/N_0$ can be related to the power $P_r$ received at the receiver as

$$E_b/N_{0,dB} = P_{r,dBm} - 10\log_{10}\frac{f_b}{B} - N_{dBm} \quad (4)$$

where $N = kTBN_F$ is the noise power, $k$ is the Boltzmann constant, $T$ is the environment temperature, $N_F$ is the noise figure of the front-end of receiving module, and

$$P_{r,dBm} = P_{t,dBm} - PL_{dB} \quad (5)$$

where the path loss $PL_{dB}$ can be referred from Figs. 7 and 8. So, at various data rates, $E_b/N_o$ can be calculated using (4) and (5) and the maximum data rate which ensures a BER of $10^{-3}$ can be derived for different transmitting electrode positions.

Fig. 16 shows the calculated bit error rate versus transmitting electrode positions. As can be seen, the positions $C_3$, $C_z$ and $F_z$ provide the best BER performance, i.e., a BER smaller than $10^{-6}$ at a date rate of 10 Mbps. When the date rate is reduced to 1.25 Mbps, except for the positions $O_1$, $T_5$ and $T_6$, the other positions still ensure a BER below $10^{-3}$. Compared to the path loss in Fig. 8, it can be found that the path loss at positions $O_1$, $T_5$ and $T_6$ is larger than that at other positions. The large path loss is the main reason of the high bit error rates. Fig. 17 shows the possible data rate ensuring $10^{-3}$ BER for various transmitting electrode positions, again, the positions $C_3$, $C_z$, $F_7$ and $F_z$ provide the fastest data rate. Even for the positions at the head back, a BER of $10^{-3}$ can still be ensured when reducing the data rate to 0.3 Mbps. Such a date rate is still possible to be used for ten-channel EEG signal transmission.

On the other hand, from (4) and (5), we can obtain the $P_t$ required to satisfy a specific BER at a specific transmitting electrode position. For example, at the position $O_1$, to obtain an $E_b/N_0$ of 10.94 dB at data rate of 10 Mbps, the transmitting power $P_t$ is required to be 0.082 mW (-10. 89 dBm). This transmitting power level obviously meets the defined level
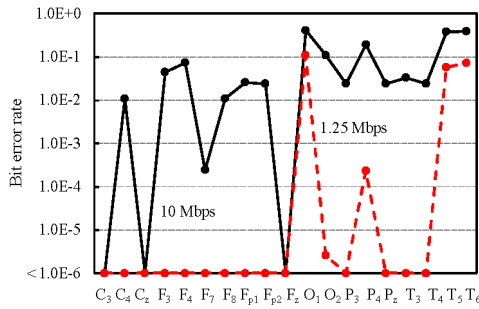
**IEEE** *Access*

W. Liao *et al.*: Path Loss Analysis and Transceiver Development for HBC-Based Signal Transmission for Wearable Robot Control



**FIGURE 16.** Bit error rate versus transmitting electrode positions.
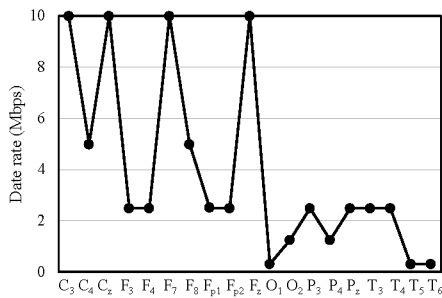


**FIGURE 17.** Data rate ensuring a BER of $10^{-3}$ versus transmitting electrode positions.



**FIGURE 18.** Block diagram of evaluation experiment of the transceiver using a bio-equivalent gel phantom.



**FIGURE 19.** Transmitted (orange) and demodulated (green) EEG signals. They almost overlap and are almost indistinguishable.

for HBC at the IEEE 802.15.6. In addition, for human safety, even if all the transmitting power of 0.082 mW is absorbed by 10 grams of human tissues, the local specific absorption rate (SAR) is only 8.2 mW/kg, much smaller than the safe limit of 2 W/kg [9].

Finally, the performance of the developed transceiver was further experimentally evaluated using a bio-equivalent gel phantom. The gel phantom was 30 - 100 cm long and had a cross-section of 6 cm × 7 cm. It was composed of glycerin, deionized water, sodium benzoate and agar [27], and approximately simulated the averaged dielectric properties of the human arm in the frequency band used. Since the basic transmission mechanism of HBC is based on electrostatic coupling as described previously, the complicated tissue structure inside the human body is not dominate. A gel phantom is therefore popularly used to simulate the human body by making it to have the same electrical properties as actual human body. This suitability of the phantom has been confirmed in [28]. As shown in Fig. 18, an EEG signal was output from a pseudo signal generator and applied to the transmitting electrode on the left side of the gel phantom. The receiving electrode was set to the right side of the phantom. The length of the gel phantom was changed from 30 cm to 100 cm to simulate a distance from the head to the wrist. Fig. 19 shows the pseudo EEG signal transmitted and the demodulated pseudo EEG signal at the length of 100 cm. They agreed well and the correlation coefficient between them was found as high as 0.95. This suggests the feasibility of the developed transceiver for EEG signal transmission. Although the waveform received at the receiver input was actually distorted from the original transmitted
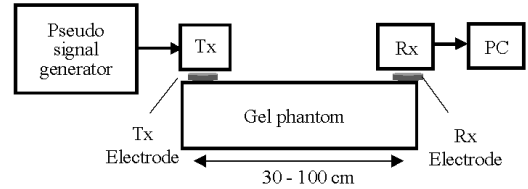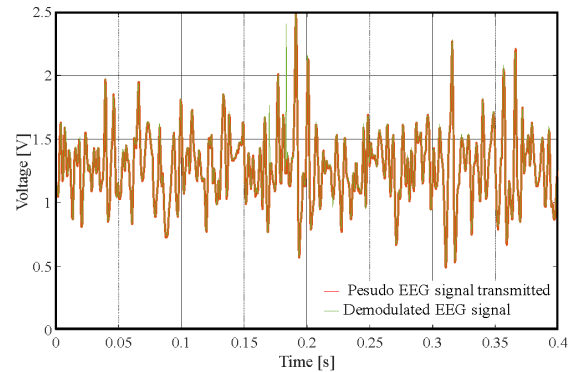
waveform because of its propagation through the human body, the appropriate demodulation recovered the EEG signal in a high accuracy. No equalization technology was used.

However, actual signal transmission along the human body may be different from the gel phantom. It can be greatly affected by individual difference. We therefore applied the developed transceiver to five human subjects to verify its actual transmission performance. Since the relationship between the EEG signal and the hand action is still under study, instead of transmitting an EEG signal from the head, we used the developed transceiver to detect the EMG signals in the arm and then transmitted them along the arm to the wrist. The EMG signals obtained from the wrist-mounted receiver were used to control a robotic hand as in [23]. The robotic hand was set to two actions: open or close the hand. The transmission experiment was performed for the five human subjects, and was repeated five times for each subject. The results show that the two actions were accurately manipulated each time.

## V. CONCLUSION

To transmit EEG signals from head to wrist in the 10-60 MHz HBC band for wearable robot control, we have theoretically clarified the transmission mechanism using a highly simplified human body model, and numerically derived the propagation characteristics using an anatomical human body model with five typical postures. Based on the analysis results, we have optimized the transmitter positions on the head, and developed an HBC-based impulse radio transceiver for signal transmission from the head to the wrist. The results have shown that the data rate can reach 10 Mbps and the BER can

W. Liao *et al.*: Path Loss Analysis and Transceiver Development for HBC-Based Signal Transmission for Wearable Robot Control

IEEE *Access*

be kept below $10^{-3}$ using the developed transceiver. Experimental validation with a bio-equivalent gel phantom has also demonstrated the usefulness of the technique by successfully transmitting a pseudo EEG signal along the artificial human arm.

The next step in this study is to combine the developed transceiver with an EEG sensor to transmit actual EEG signals and use them to control a wearable robot.

## REFERENCES

[1] J. Wang and Q. Wang, *Body Area Communication*. Hoboken, NJ, USA: Wiley-IEEE, 2012.

[2] T. G. Zimmerman, "Personal area networks: Near-field intrabody communication," *IBM Syst. J.*, vol. 35, nos. 3–4, pp. 609–617, 1996.

[3] H. Baldus, S. Corroy, A. Fazzi, K. Klabunde, and T. Schenk, "Human-centric connectivity enabled by body-coupled communications," *IEEE Commun. Mag.*, vol. 47, no. 6, pp. 172–178, Jun. 2009.

[4] E. Monton, J. F. Hernandez, J. M. Blasco, T. Herve, J. Micallef, I. Grech, A. Brincat, and V. Traver, "Body area network for wireless patient monitoring," *IET Commun.*, vol. 2, no. 2, pp. 215–222, Feb. 2008.

[5] F. Chen, Z. Li, C. L. Philip Chen, and S. Agaian, "Introduction to the special issue on human cooperative wearable robotic systems," *IEEE Robot. Autom. Lett.*, vol. 3, no. 1, pp. 466–468, Jan. 2018.

[6] L. Randazzo, I. Iturrate, S. Perdikis, and J. D. R. Millan, "Mano: A wearable hand exoskeleton for activities of daily living and neurorehabilitation," *IEEE Robot. Autom. Lett.*, vol. 3, no. 1, pp. 500–507, Jan. 2018.

[7] J. Wang, "Wide band human body communication technology for wearable and implantable robot control," *IEICE Trans. Commun.*, vol. 103, no. 6, pp. 628–636, Jun. 2020.

[8] M. Chen, J. Zhou, G. Tao, J. Yang, and L. Hu, "Wearable affective robot," *IEEE Access*, vol. 6, pp. 64766–64776, Oct. 2018.

[9] *IEEE Standard for Local and Metropolitan Area Network-Part 15.6: Wireless Body Area Networks*, IEEE Std 802.15.6-2012, Feb. 2012.

[10] J. Wang, Y. Nishikawa, and T. Shibata, "Analysis of on-body transmission mechanism and characteristic based on an electromagnetic field approach," *IEEE Trans. Microw. Theory Techn.*, vol. 57, no. 10, pp. 2464–2470, Oct. 2009.

[11] J. Park, H. Garudadri, and P. P. Mercier, "Channel modeling of miniaturized battery-powered capacitive human body communication systems," *IEEE Trans. Biomed. Eng.*, vol. 64, no. 2, pp. 452–462, Feb. 2017.

[12] (2015). *The Radio Use Website*. (in Japanese). [Online]. Available: http://www.tele.soumu.go.jp/j/ref/material/rule/

[13] J. Wang, T. Fujiwara, T. Kato, and D. Anzai, "Wearable ECG based on impulse-radio-type human body communication," *IEEE Trans. Biomed. Eng.*, vol. 63, no. 9, pp. 1887–1894, Sep. 2016.

[14] H. M. Barlow and J. Brown, *Radio Surface Waves*. Oxford, U.K.: Oxford Univ. Press, 1962.

[15] T. Nagaoka, S. Watanabe, K. Sakurai, E. Kunieda, S. Watanabe, M. Taki, and Y. Yamanaka, "Development of realistic high-resolution whole-body voxel models of Japanese adult males and females of average height and weight, and application of models to radio-frequency electromagnetic-field dosimetry," *Phys. Med. Biol.*, vol. 49, no. 1, pp. 1–15, Jan. 2004.

[16] C. Gabriel, "Compilation of the dielectric properties of body tissues at RF and microwave frequencies," Brooks Air Force, San Antonio, TX, USA, Tech. Rep. AL/OE-TR-1996-0037, 1996.

[17] N. Cho, J. Yoo, S.-J. Song, J. Lee, S. Jeon, and H.-J. Yoo, "The human body characteristics as a signal transmission medium for intrabody communication," *IEEE Trans. Microw. Theory Techn.*, vol. 55, no. 5, pp. 1080–1086, May 2007.

[18] J. Bae, H. Cho, K. Song, H. Lee, and H.-J. Yoo, "The signal transmission mechanism on the surface of human body for body channel communication," *IEEE Trans. Microw. Theory Techn.*, vol. 60, no. 3, pp. 582–593, Mar. 2012.

[19] S. Maity, M. He, M. Nath, D. Das, B. Chatterjee, and S. Sen, "Bio-physical modeling, characterization, and optimization of electro-quasistatic human body communication," *IEEE Trans. Biomed. Eng.*, vol. 66, no. 6, pp. 1791–1802, Jun. 2019.

[20] S. Maity, K. Mojabe, and S. Sen, "Characterization of human body forward path loss and variability effects in voltage-mode HBC," *IEEE Microw. Wireless Comp. Lett.*, vol. 28, no. 3, pp. 266–268, Mar. 2018.

[21] M. H. Seyedi and D. T. H. Lai, "Effect of limb joints and limb movement on intrabody communications for body area network applications," *J. Med. Biol. Eng.*, vol. 34, no. 3, pp. 276–283, 2014.

[22] J. Wang, K. Nomura, H. Narita, F. Ito, D. Anzai, J. Bergsland, and I. Balasingham, "Development and *in vivo* performance evaluation of 10–60-MHz band impulse-radio-based transceiver for deep implantation having 10 Mbps," *IEEE Trans. Microw. Theory Techn.*, vol. 66, no. 9, pp. 4252–4260, Sep. 2018.

[23] H. Ando, Y. Murase, D. Anzai, and J. Wang, "Wireless control of robotic artificial hand using myoelectric signal based on wideband human body communication," *IEEE Access*, vol. 7, pp. 10254–10262, Jan. 2019.

[24] M. Shinagawa, M. Fukumoto, K. Ochiai, and H. Kyuragi, "A near-field-sensing transceiver for intrabody communication based on the electrooptic effect," *IEEE Trans. Instrum. Meas.*, vol. 53, no. 6, pp. 1533–1538, Dec. 2004.

[25] S.-J. Song, N. Cho, S. Kim, J. Yoo, S. Choi, and H.-J. Yoo, "A 0.9 V 2.6 mW body-coupled scalable PHY transceiver for body sensor applications," in *IEEE Int. Solid-State Circuits Conf. (ISSCC) Dig. Tech. Papers*, San Francisco, CA, USA, Feb. 2007, pp. 366–609.

[26] J. G. Proakis and M. Salehi, *Digital Communications*. New York, NY, USA: McGraw-Hill, 2008.

[27] K. Ito, H. Kawai, and K. Saito, "State of the art and future prospects of biological tissue-equivalent phantoms," *Trans. IEICE*, vol. 85, no. 5, pp. 582–596, May 2002.

[28] J. Wang, R. Nakaya, K. Sato, D. Anzai, O. Fujiwara, and F. Amemiya, "Development of an immunity test system with a pseudo biosignal generator for wearable devices and application to the ESD test of an artificial hand," *IEEE Trans. Electromagn. Compat.*, vol. 61, no. 1, pp. 73–81, Feb. 2019.

**WEI LIAO** received the B.E. degree in electronic information engineering from Nanchang University, Nanchang, China, in 2003, and the M.E. and D.E. degrees from East China Normal University, Shanghai, China, in 2007 and 2010, respectively, both in communication and information system. From 2003 to 2004, she was a Lecturer with the Department of Information Engineering, Jiangxi University of Technology, Ganzhou, China. From 2011 to 2016, she was a Postdoctoral Research Associate with the Nagoya Institute of Technology, Nagoya, Japan. She is currently an Associate Professor with the School of Electric and Electronic Engineering, Shanghai University of Engineering Science, Shanghai. Her research interests include biomedical communications and electromagnetic compatibility.

**KOKI MURAMATSU** received the B.E. and M.E. degrees in electrical and electronic engineering from the Nagoya Institute of Technology, Nagoya, Japan, in 2018 and 2020, respectively. He was a Graduate Student with the Nagoya Institute of Technology, where he was involved in the development of wearable transceiver. He is currently with Murata Manufacturing Company Ltd., Japan.

**JIANQING WANG** (Fellow, IEEE) received the B.E. degree in electronic engineering from the Beijing Institute of Technology, Beijing, China, in 1984, and the M.E. and D.E. degrees in electrical and communication engineering from Tohoku University, Sendai, Japan, in 1988 and 1991, respectively. He was a Research Associate with Tohoku University, and a Senior Engineer with Sophia Systems Company Ltd. In 1997, he joined the Nagoya Institute of Technology, Nagoya, Japan, where he has been a Professor, since 2005. He has authored *Body Area Communications: Channel Modeling, Communication Systems, and EMC (Wiley-IEEE, 2012)*. His current research interests include biomedical communications and electromagnetic compatibility. He received the IEEE EMCS Technical Achievement Award in 2019.

• • •